19th Brazilian Congress of Thermal Sciences and Engineering
November 06th-10th, 2022, Bento Gonçalves - RS - Brazil

ENC-2022-0022
PERFORMANCE MAPPING OF A VAPOR COMPRESSION SYSTEM FOR DUAL-ZONE VEHICULAR AIR CONDITIONING APPLICATIONS

Pedro Augusto Bruggemann
Gabriel Longen Podgaietsky
Christian Johann Losso Hermes
POLO Labs, Departament of Mechanical Engineering, Federal University of Santa Catarina, Florianópolis, SC, Brazil
pedro@polo.ufsc.br

Abstract. *The present paper is aimed at mapping the thermodynamic performance of a mechanical vapor compression cycle designed for dual-zone vehicular air conditioning. To this end, two purpose-built closed-loop wind tunnel facilities were designed and constructed, one for the condenser unit and another for the two evaporator units (cockpit and cabin). Experiments were carried out for different thermal loads by varying the indoor temperature. The experimental data was assessed by means of a thermodynamic approach that splits the overall (second-law) refrigeration efficiency into two terms, namely internal and external efficiencies that account for the thermodynamic losses that take place respectively inside the refrigeration loop and at the airside of the finned-tube heat exchangers. The internal efficiency, in turn, was divided into two other terms to identify the thermodynamic irreversibilities in the compressor and also in the other components of the cycle. Finally, the compressor efficiency was separated into two other ones to account for the electromechanical and thermodynamic losses in this component. To illustrate the methodology, a sensitive analysis of the condenser airflow, was carried out exploring the consequences of the UA variation on the arrangement performance.*

Keywords: *air conditioning, mechanical vapor compression, experimentation, thermal analysis*

1. INTRODUCTION

The mechanical vapor compression cycle has been largely adopted in automotive vehicles for air conditioning purposes. There are essentially two cycle architectures used in vehicular systems. In both, the refrigeration system is comprised of four main components: compressor, condenser, expansion device and evaporator. The compressor and the expansion device keep refrigerant at low pressure in the evaporator and at high pressure in the condenser, which in turn exchange heat with the indoor and the outdoor environments, respectively. According to Shah (2009), the differences between these two basic architectures rely on the type of expansion device (orifice tube or thermostatic expansion valve) and refrigerant charge reservoir (liquid receiver or suction accumulator), as depicted in Fig. 1.

In the OT/AD (orifice tube/accumulator drier) cycle, an orifice tube, with fixed restriction, is used as the expansion device, whereas a suction accumulator is placed at the evaporator outlet to retain the liquid, thus avoiding compressor slugging. In the TXV/RT (thermostatic expansion valve/receiver drier) architecture, a receiver is placed at the condenser outlet to prevent the admission of vapor bubbles into the TXV, used as the expansion device. In this loop, superheated refrigerant at low pressure (1) is suctioned by the compressor and then discharged in the condenser (2), which consumes electric power. Then, vapor refrigerant is de-superheated and undergoes condensation while heat is released to the outdoor environment, so that either two-phase refrigerant or subcooled liquid can be found at the receiver inlet (3). Liquid refrigerant (4) then flashes in the expansion device so that a two-phase mixture flows through the evaporator (5), removing heat from the indoor environment while liquid refrigerant turns into vapor until a certain degree of superheating, which is ruled by the TXV, is achieved.

Although the literature regarding single-zone automotive air conditioning systems is abundant (see, for instance, Kaynakli and Horuz, 2003; Tian et al., 2005; Zheng et al., 2014; Cho and Park, 2016), studies aiming at dual-zone applications are scarce (Ahn et al., 2015). In this sense, the present paper is aimed at putting forward an experimental methodology for mapping the thermodynamic performance of a dual-zone air conditioning vapor compression system for vehicular applications.

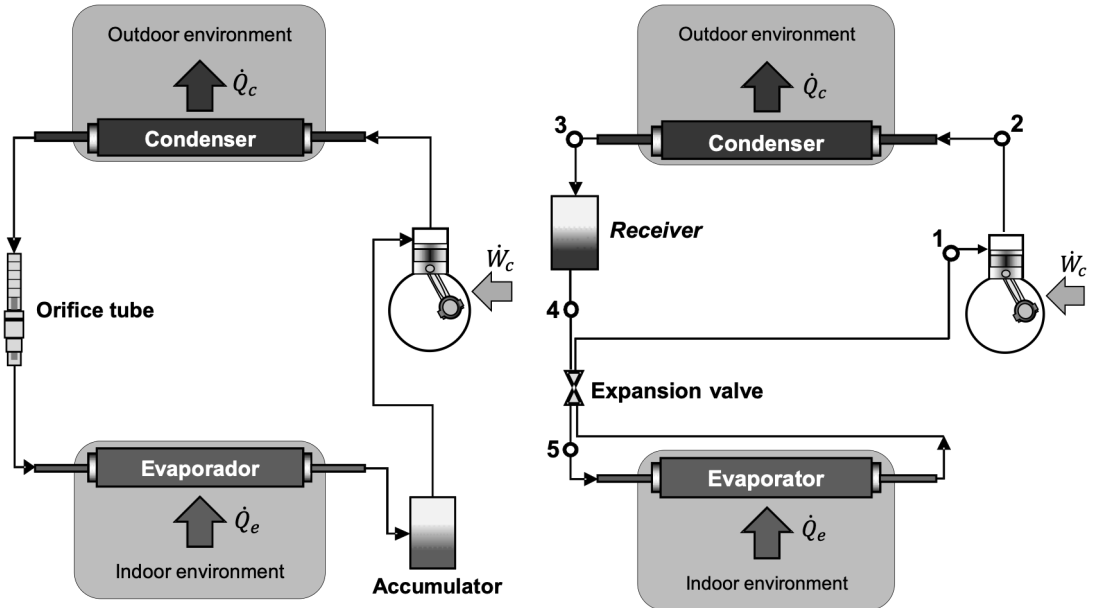

Figure 1. **Typical refrigeration cycle architectures of vehicular air conditioners: OT-AD (left) and TXV-RT (right)**

2. EXPERIMENTAL SETUP

The VCS under analysis consists of a dual-evaporator refrigeration cycle, one for the cockpit (driver) and another for the cabin (passengers). The cycle is comprised of an open-type compressor, which is responsible for controlling the evaporating temperature by means of variable piston displacement. The condenser and the evaporators are fan-supplied tube-fin heat exchangers made of aluminum fins and copper tubes. A receiver is placed at the condenser outlet, while thermostatic valves are installed at the inlet of each evaporator to control the superheating degree. Refrigerant R134a is adopted as the working fluid. The experimental apparatus consists of a calorimetric setup comprised of two closed-loop wind-tunnel facilities, one for the condenser and another for the evaporators, both designed based on the recommendations of standards ANSI / ASHRAE 41.2 (1987) and ANSI / ASHRAE 33 (2000). The evaporator wind-tunnel has two test sections (double deck), thus allowing individual control of the air flow supplied for each evaporator. In order to keep the original internal volume of the VCS, the refrigeration loop was installed with the very same refrigerant lines (hoses that connect one component to the other) employed in the vehicle. A schematic representation is illustrated in Fig. 2.

To mitigate the heat exchange between the test section and the external environment, the wind tunnels were built with 50-mm thick walls filled with insulating material (rockwool). The condenser wind-tunnel test section is 2.8 m long and has an internal cross section of 900 x 900 mm, where the condenser (g) and two flow homogenizers (f) (note that just the one at the condenser upstream is illustrated in Fig. 2) are placed. Also, two grids comprised of 9 thermocouples each are installed at the entrance and exit of the test section for air temperature measurements. Static pressure taps (4 for each section) are also available at the condenser inlet and outlet. In the other branch, the air passes through a perforated screen (e) placed upstream of a nozzle (d) used to measure the air flow rate. The air stream is then cooled down by an auxiliary cooling system (c), and re-heated by PID-controlled electric heaters (b). The air flow is supplied by a variable-speed radial fan (a).

The evaporator wind-tunnel is quite similar to the condenser one, despite the double deck test section designed to accommodate both cabin and cockpit evaporators. The test section is also 2.8 m long and has internal cross sections of 500 x 700 mm for each deck. Once again, two temperature homogenizers and two thermocouple grids are installed at the entrance and exit of the test sections together with humidity transducers with a measurement uncertainty of ± 1.5%. All temperatures are measured using T-type thermocouples with an uncertainty of ± 0.2ºC. To reduce signal fluctuations in the measurements of the air temperatures, the thermocouple joints are inserted and brazed into copper cylinders with 10-mm height and 10-mm diameter. In this assembly, the nozzles (h) and (i) are place downstream the test section. The air temperature is set by a PID-controlled electric heater (j). The air is blown by a single variable-speed fan (k), whereas the air flow supplied to each test section is controlled by two dampers arranged in parallel (l).

The pressure drops in the air circuit are measured using differential pressure transducers with an uncertainty of ± 0.5% full scale. The volumetric air flow rates are calculated as a function of the pressure difference in the nozzles also measured by differential pressure transducers. Since the thermal insulation does not completely prevent heat transfer, which can lead to small errors in the calculation of heat transfer rates in the condenser and evaporators, the overall thermal conductances (UA) of the test sections of both wind-tunnel were determined from reverse heat leakage tests (Da Silva et al., 2011).

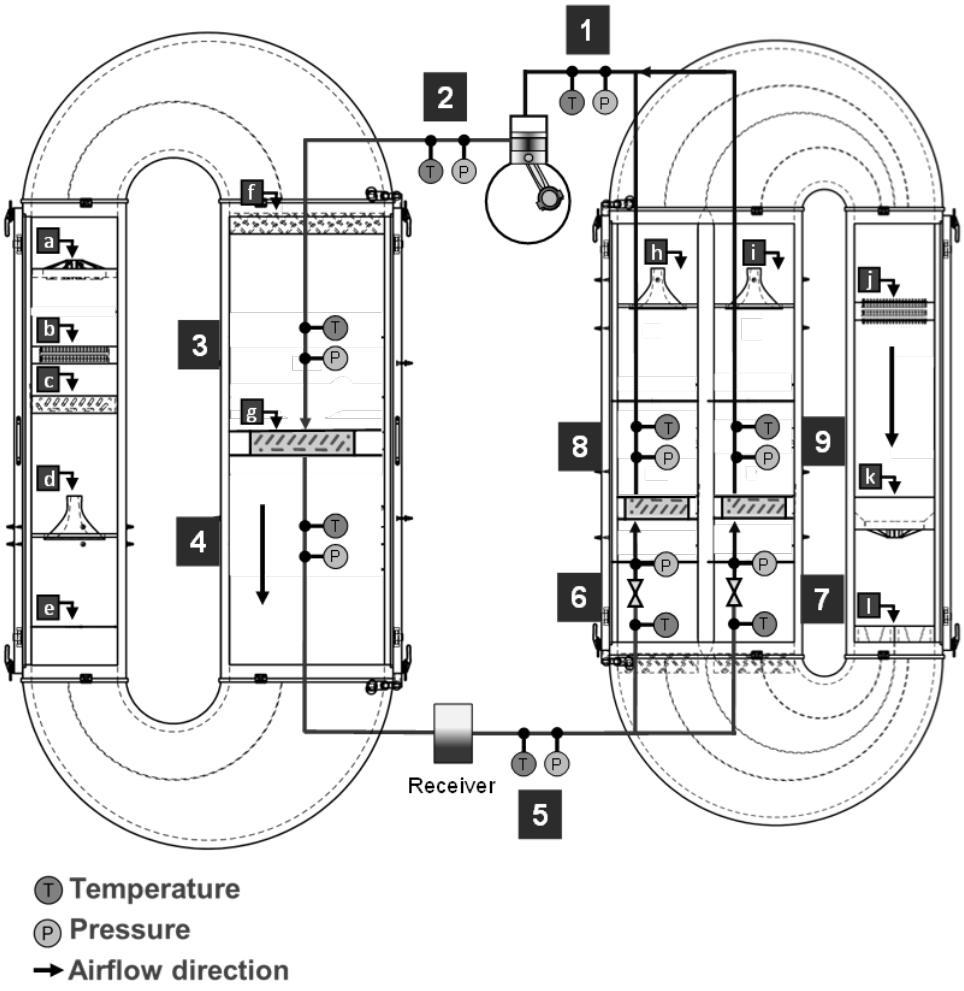

Figure 2. **Schematic representation of the experimental setup and instrumentation**

Additionally, contact thermocouples are installed on the compressor walls, the condenser inlet and outlet tubes, the receiver outlet, the expansion valve inlets and the evaporator outlet. To avoid electrical interference, a Kapton film was applied between the thermocouples and the surface of the refrigerant lines. Seven absolute pressure transducers are also installed along the refrigeration loop to determine the suction and discharge pressures of the compressor, in addition to the pressure drops taking place in the heat exchangers. A summary of the refrigerant loop instrumentation is depicted in Fig. 3 by means of pressure-enthalpy and temperature-entropy diagrams, where one can see the thermodynamic states at the compressor suction (1) and discharge (2), at condenser inlet (3) and outlet (4), at the entrance of the TXVs (5), and at the cockpit (6, 8) and cabin (7, 9) evaporators (inlet, outlet).

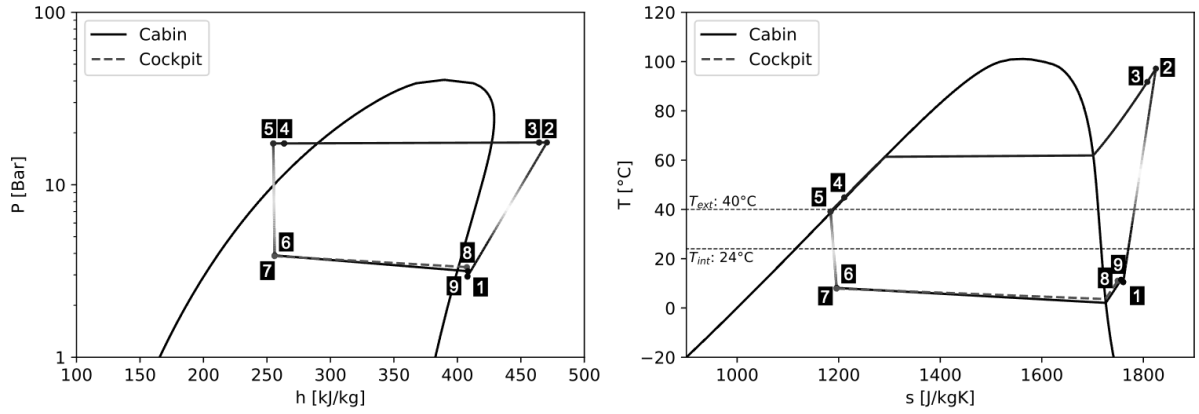

Figure 3. **Experimental data representation in pressure-enthalpy (left) and temperature-entropy (right) diagrams**

The data acquisition system is comprised of four temperature input modules used together with two voltage and two current modules with eight channels each, responsible for the reading signals from absolute pressure, differential pressure and relative humidity transducers. For each measured variable, the data acquisition program computes the maximum standard deviation of the last 600 readings and verifies if the steady-state condition has been achieved, which is based on a linear fit of all datapoints measured in an interval of 10 minutes. The test is considered at steady-state regime when the maximum slope is lower than three standard deviations.

3. DATA REDUCTION

Raw data of temperature, humidity, pressure and air flow rate are obtained by means of the instrumentation described in the previous section. Based on such information, it is possible to calculate the key parameters for mapping the performance thermodynamic of the system. For instance, the heat duty of the condenser can be determined using the following energy balance on the air side:

$$\dot{Q}_{cnd} = \left(\rho \dot{V} c_p\right)_{cnd} \left(T_{cnd,out} - T_{cnd,in}\right) \tag{1}$$

where ρ is the density and c_p is the specific heat of dry air, both evaluated at the average temperature of the test section, $\dot{V}$ is the air flow rate measured at the nozzle, and $T_{cnd,in}$ and $T_{cnd,out}$ are, respectively, the air temperature at the condenser inlet and outlet sections. For the evaporators, both sensible and latent heat are present, so that their cooling capacities can be determined by the following energy balances on the cabin and cockpit evaporators:

$$\dot{Q}_{ca} = \left(\rho \dot{V}\right)_{ca} \left(h_{ca,in} - h_{ca,out}\right) \tag{2}$$

$$\dot{Q}_{ck} = \left(\rho \dot{V}\right)_{ck} \left(h_{ck,in} - h_{ck,out}\right) \tag{3}$$

where ρ is the density of dry air, whereas h_{in} and h_{out} are, respectively, the enthalpy of moist air at the inlet and outlet of the cabin (ca) and cockpit (ck) evaporators, in [kJ/kg$_{dry}$]. Therefore, the cycle COP can be calculated as follows:

$$COP = \frac{\dot{Q}_{evp}}{\dot{W}_{cmp}} \tag{4}$$

where $\dot{Q}_{evp} = \dot{Q}_{ca} + \dot{Q}_{ck}$ is the cooling capacity of the system, whereas the electric power supplied to the compressor is calculated from $\dot{W}_{cmp} = iV$, where i is the amperage and V the voltage.

The thermodynamic mapping starts with the definition of the overall refrigeration efficiency (or second-law efficiency), calculated as follows (Gosney, 1982):

$$\eta_{ref} = \frac{COP}{COP_{rev}} \tag{5}$$

where COP_{rev} is the coefficient of performance of a reversible (Carnot) refrigerator, calculated from:

$$COP_{rev} = \frac{T_{id}}{T_{od} - T_{id}} \tag{6}$$

where T_{od} and T_{id} are the temperatures of the hot (outdoor) and cold (indoor) reservoirs. Introducing $COP_{int,rev}$, the coefficient of performance of an endoreversible refrigerator – i.e., the COP of an internally reversible cycle operating between the condensing, T_{cnd}, and the evaporating, T_{evp}, temperatures of the real cycle:

$$COP_{int,rev} = \frac{T_{evp}}{T_{cnd} - T_{evp}} \tag{7}$$

Thus, the overall refrigeration efficiency can be split into two terms, namely internal and external efficiencies (Hermes and Barbosa, 2011), as follows:

$$\frac{COP}{COP_{rev}} = \frac{COP}{COP_{int,rev}} \frac{COP_{int,rev}}{COP_{rev}} \tag{8}$$

Alternatively, one can write $\eta_{ref} = \eta_{int}\eta_{ext}$, where

$$\eta_{int} = \frac{COP}{COP_{int,rev}} \tag{9}$$

$$\eta_{ext} = \frac{COP_{int,rev}}{COP_{rev}} \tag{10}$$

A close inspection of equations (9) and (10) reveals that η_{int} accounts for the losses taking place inside the refrigeration loop (e.g., electromechanical and thermodynamic losses in the compressor, refrigerant-side pressure drops in the heat exchanger coils, non-isentropic throttling in the expansion devices), while η_{ext} stands for the external losses of the cycle (basically, heat transfer with non-zero temperature difference in the condenser and the evaporators). Defining $\Delta T_{evp} \equiv T_{id} - T_{evp}$ and $\Delta T_{cnd} \equiv T_{cnd} - T_{od}$, and replacing T_{cnd} and T_{evp} in eq. (7), one can show that:

$$COP_{int,rev} = \frac{T_{id} - \Delta T_{evp}}{T_{od} - T_{id} + \Delta T_{cnd} + \Delta T_{evp}} \tag{11}$$

The thermodynamic mapping goes on by splitting η_{int} into two other terms, so that $\eta_{int} = \eta_{cmp}\eta_{oth}$, where η_{cmp} is the global efficiency of the compressor, calculated from (Gosney, 1982):

$$\eta_{cmp} = \frac{\dot{m}(h_{2,s} - h_1)}{\dot{W}_{cmp}} \tag{12}$$

where η_{oth} is the efficiency of the remaining (other) components of the cycle, including (but not limited to) the thermodynamic losses due to pressure drop in the heat exchangers and the irreversible throttling in the expansion devices. In eq. (12), h_1 is the enthalpy of the refrigerant at the compressor inlet, $h_{2,s}$ is the enthalpy of the refrigerant after a hypothetical isentropic compression, and $\dot{m}$ is the mass flow rate of refrigerant obtained from an energy balance in the refrigerant side of the condenser, as follows:

$$\dot{m} = \frac{\dot{Q}_{cnd}}{h_3 - h_4} \tag{13}$$

where h_3 and h_4 are the enthalpies of the refrigerant at the condenser inlet and outlet, respectively. Furthermore, the global compressor efficiency η_{cmp} can also be split into two terms, $\eta_{cmp} = \eta_{th}\eta_{em}$, namely the isentropic compression efficiency, η_{th}, and the electromechanical efficiency of the compressor, η_{em}. The latter accounts for the amount of electrical power that is effectively converted into refrigerant enthalpy, thus quantifying the electromechanical losses in the compressor (e.g., control board, electric motor, transmission mechanism, lubricating bearings, valves),

$$\eta_{em} = \frac{\dot{m}(h_2 - h_1)}{\dot{W}_{cmp}} \tag{14}$$

whereas the isentropic efficiency stands for the non-idealities of the thermodynamic compression itself, being calculated as follows (Gosney, 1982):

$$\eta_{th} = \frac{h_{2,s} - h_1}{h_2 - h_1} \tag{15}$$

where h_2 is the enthalpy of the refrigerant measured at the compressor discharge. Figure 4 illustrates the efficiency deployment from the system-level to the compressor-level showing the thermodynamic irreversibilities taking place in the VCS as a whole. In this work, the thermodynamic properties of refrigerant R134a are obtained from the Coolprop software (Bell et al., 2014).

4. RESULTS

Tests were carried out for three different indoor temperatures: 18 (low), 24 (mid) and 35ºC (high), while the outdoor temperature was held constant at 40ºC. Fig. 6 explores the thermodynamic efficiencies of the system (internal, external and overall) for different indoor temperatures. One should bear in mind that the internal efficiency takes into account the viscous losses in the refrigerant flow through the heat exchangers and hoses as well as the non-idealities of the

compression process, while the external efficiency indicates opportunities for improvements in the heat transfer with the air. One can note that, although the internal and the external efficiencies have similar magnitudes (~30%) for the low indoor temperature, as the ΔTs are not so large at this condition, the difference increases significantly as the indoor temperature increases, so that the external efficiency becomes dominant for higher indoor temperatures, while the internal efficiency practically does not vary as a result of the low variation of the COP with the indoor temperatures (see Fig. 6).

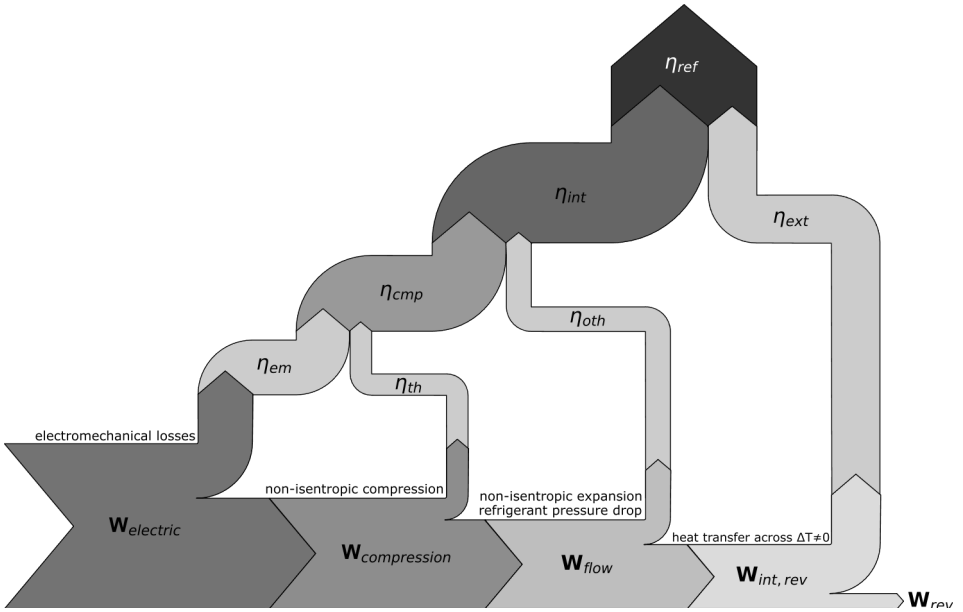

Figure 4. **Deployment of the thermodynamic efficiencies from the system-level to the component-level**

Indeed, the external efficiency of the system decreases dramatically with the increase of the indoor temperature, which can be explained by the drastic rise in the air-coil temperature difference experienced by both the evaporators and the condenser, as illustrated in Fig. 5. According to equation (10), increasing ΔT_{evp} and ΔT_{cnd} leads to a reduced $COP_{int,rev}$, which in turn increases η_{int} (see eq. 9) and decreases η_{ext} (see eq. 10). As a net effect, the COP of the system is reduced from ~10% to ~2.5% of the COP of an ideal (Carnot) refrigerator when the indoor temperature rises from 18 to 35ºC. Therefore, opportunities to improve the system performance lie not only on increasing the heat exchanger conductances but also on enhancing the control strategies.

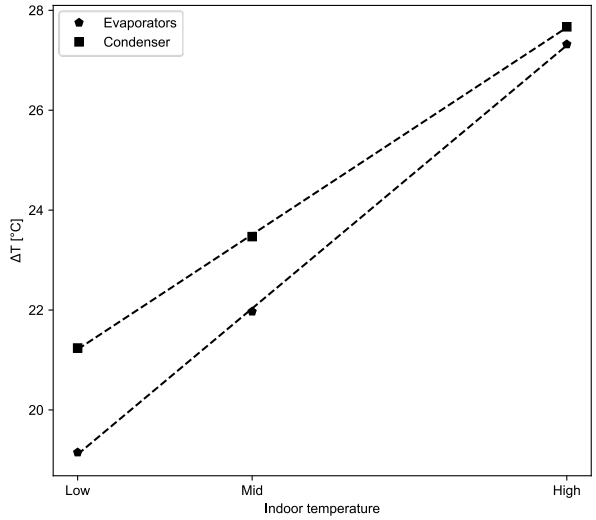

Figure 5: Temperature differences in the condenser and evaporators as a function of the indoor temperature

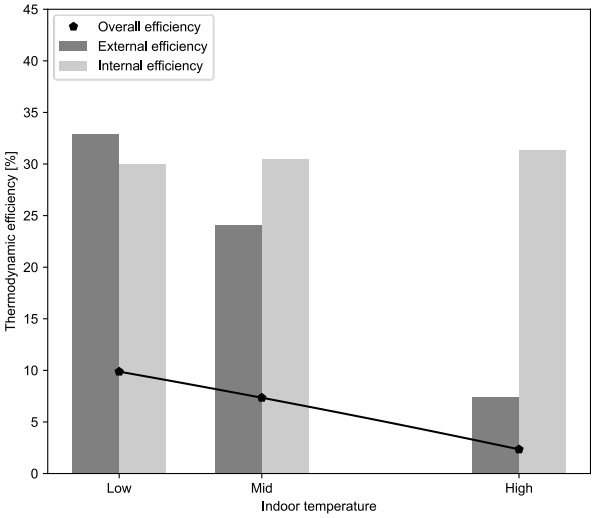

Figure 6: Efficiency deployment at system-level: internal, external and overall

A close inspection of the irreversibilities taking place inside the refrigeration loop is possible with the help of Fig. 7, where the internal efficiency, that experienced a slight variation with the indoor temperature, is split into two terms, one related to the compressor efficiency and another to the other components of the refrigeration loop. It is clear that the former (~37%) overrules the latter (~81%). Figure 8, in turn, split the compressor efficiency into two others, one related

to the amount of enthalpy delivered to the refrigerant through an ideal compression, and another related to the losses in the electromechanical components of the compressor. It can be seen that for both the isentropic and eletromechanical efficiency there is a negligible variation with the indoor temperature, therefore the global compressor efficiency remains practically constant too.

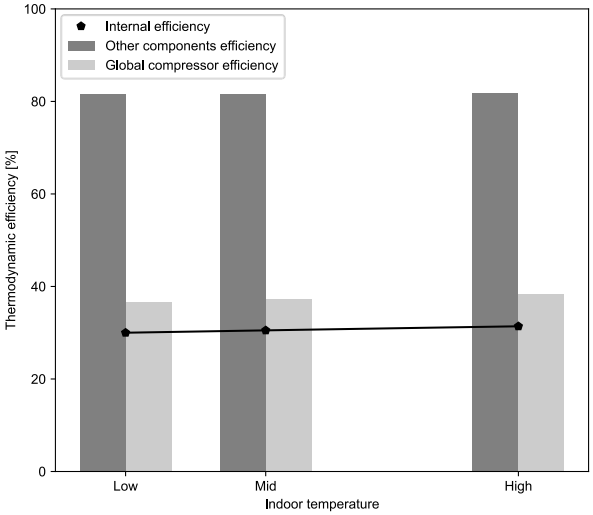

Figure 7: Efficiency deployment for an endoreversible cycle: internal, compressor and other components

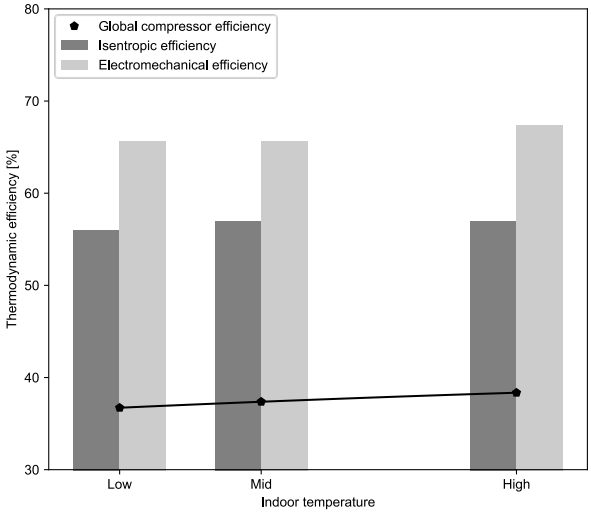

Figure 8: Efficiency deployment for the compressor: isentropic, electro-mechanical, and global

To better explore the meaning and behavior of the efficiencies, the air flow over the condenser was varied and the performance of the system was evaluated. In the graph of the Fig. 9, it is possible to notice that the expected behavior of the UA value is observed for the condensers, with an asymptotic growth of the conductance as a function of the air flow. The UA of the evaporators is shown in the same figure, note that the UA of the evaporators remains constant as the air flow over the condenser is varied throughout the tests, which is in line with the expected behavior, since the phenomenon of heat exchange is dominated by external convection in the air, which is not changed to the evaporators.

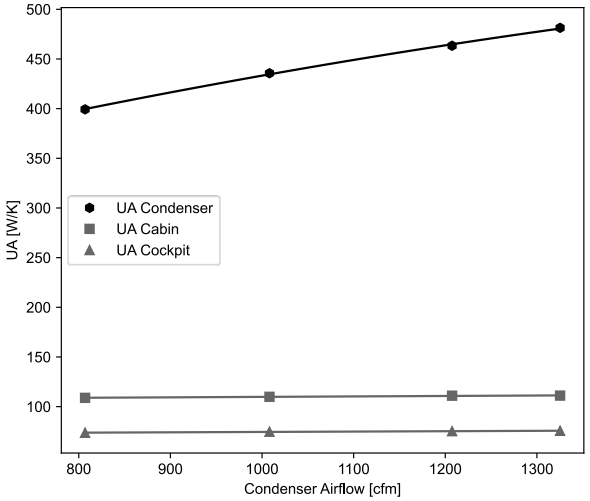

Figure 9: Heat exchanger UA coefficients as a function of the air flow rate

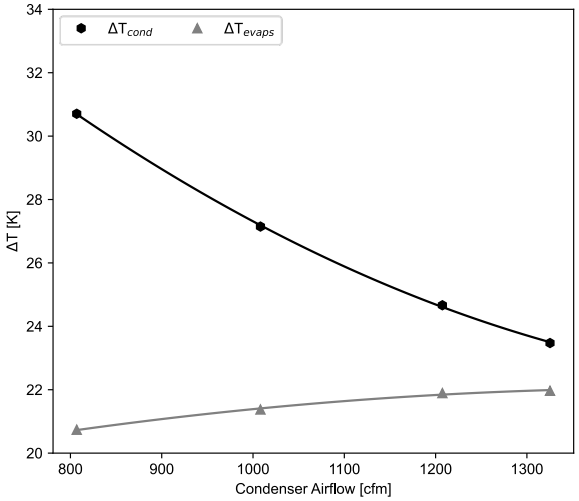

Figure 10: Temperature differences in the condenser and evaporators

In Fig. 11, it is observed that the increase of UA of the condenser generated a smaller difference in temperature over the condenser, defined as the difference between the condensation temperature and the air inlet temperature. For the evaporators, a little increase is observed between the temperature differences, inlet air temperature minus evaporation temperature. The slight increase in the temperature difference over the evaporator is due to the reduction in the condensation temperature with the increase in the air flow over the condenser, which provides a lower evaporation temperature. This effect, combined with the maintenance of the evaporators UAs, leads to a little increase in the refrigeration capacity as the condenser airflow grows. The reduction in the temperature difference over the condenser, in turn, has the consequence of raise the external efficiency, as observed in Fig. 12.

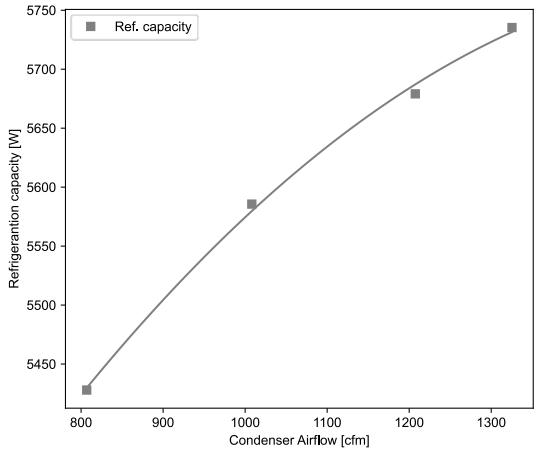

Figure 11: Cooling capacity as a function of the air flow rate

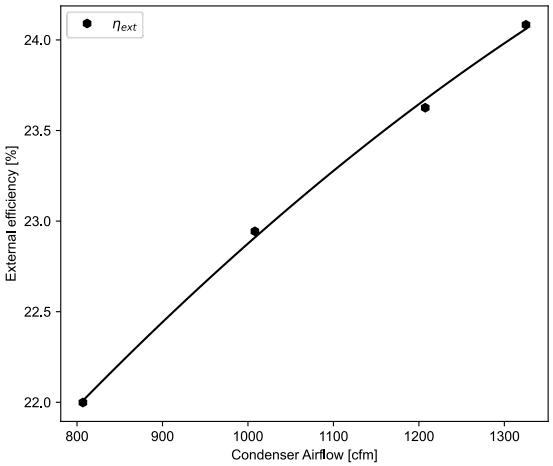

Figure 12: Cooling capacity as a function of the air flow rate

5. CONCLUSIONS

An experimental characterization of a dual-zone vapor compression air conditioning systems for vehicular applications is presented. To this end, two closed-loop wind-tunnel facilities were designed and constructed, one for the condenser and another for the two evaporators (cabin and cockpit), allowing a strict control of the temperature and flow rate of the air streams at the indoor and outdoor environments. A methodology for mapping the system performance was put forward purely on thermodynamic grounds. Tests were carried out for three different indoor temperatures, while the outdoor temperature was held fixed. A sensitive analysis of the condenser airflow, was carried out exploring the consequences of the UA variation on the arrangement performance. The key conclusions of this work are summarized as follows:

- While the internal efficiency remains fairly constant, the external efficiency decreases with the indoor temperature. The difference between them is quite small for 18ºC, but increases substantially for 35ºC, with the external losses becoming dominant and dropping the overall efficiency from 10 to 2.5%.
- The internal efficiency is ruled by the compressor, whose efficiency is ~37% whereas the efficiency of the other components of the cycle is ~81%, being both fairly constant with the indoor temperature.
- On the one hand, replacing of the compressor by a more efficient one seems to be an effective solution for improving the system performance at low indoor temperatures. On the other hand, performance enhancements at high indoor temperatures can be achieved not only by adopting heat exchangers with higher conductivities but also by revisiting the control logic.
- The condenser airflow directly impacts your UA. This effect generates a reduction in the temperature difference over the condenser and a slight increase in the temperature difference over the evaporators. Which in turn leads to a slight increase in refrigeration capacity (~5%) and an increase in external efficiency (~9.5%).

6. NOMENCLATURE

c_p	[J kg^{-1}K^{-1}]	Specific heat
COP	[-]	COP of a real cycle
COP_{rev}	[-]	COP of a reversible (Carnot) cycle
$COP_{int,rev}$	[-]	COP of an internally reversible cycle
h	[J kg^{-1}]	Specific enthalpy
p	[Pa]	Pressure
$\dot{Q}$	[W]	Heat transfer rate
T	[K]	Temperature
UA	[W K^{-1}]	Thermal conductance
$\dot{V}$	[m³ s^{-1}]	Air flow rate
$\dot{W}$	[W]	Compression power

Greek

η_{ref}	[-]	Overall refrigeration (second-law) efficiency
η_{int}	[-]	Internal (endoreversible) efficiency
η_{ext}	[-]	External efficiency

η_{cmp}	[-]	Global compressor efficiency
η_s	[-]	Isentropic compression efficiency
η_{em}	[-]	Electromechanical compressor efficiency
η_{oth}	[-]	Cycle (other components than compressor) efficiency
ρ	[kg m^{-3}]	Specific mass of dry air

Subscripts

ca	Cabin
ck	Cockpit
cmp	Compressor
cnd	Condenser
evp	Evaporator
ext	External
id	Indoor
in	Inlet
int	Internal
od	Outdoor
out	Outlet

7. ACKNOWLEDGMENT

Funding was provided by the National Institutes of Science and Technology (INCT) Program (CNPq Grant No. 404023/2019-3; FAPESC Grant No. 2019TR0846).

8. REFERENCES

Ahn, J. H., Kang, H., Lee, H. S., Kim, Y., Performance characteristics of a dual-evaporator heat pump system for effective dehumidifying and heating of a cabin in electric vehicles, Appl. Therm. Eng. 146 (2015) 29-37

ASHRAE 33, Method of Testing Forced Circulation Air Cooling and Air Heating Coils, American Society of Heating, Refrigeration and Air Conditioning Engineers, Atlanta-GA, USA, 2000

ASHRAE 41.2, Standard Methods for Laboratory Airflow Measurement, American Society of Heating, Refrigeration and Air Conditioning Engineers, Atlanta-GA, USA, 1987

Bell I.H., Wronski J., Sylvain Q., Lemort V., Pure and Pseudo-pure Fluid Thermophysi-cal Property Evaluation and the Open-Source Thermophysical Property Library Cool-Prop, Industrial & Eng. Chem. Research 53 (2014) 2498-2508

Cho, H., Park, C., Experimental investigation of performance and exergy analysis of automotive air conditioning systems using refrigerant R-1234yf at various compressor speeds, Appl. Therm. Eng. 101 (2016) 30-37

Da Silva, D.L., Hermes, C.J.L., Melo, C., Experimental Study of Frost Accumulation on Fan-Supplied Tube-Fin Evaporators, Applied Thermal Engineering 31 (2011) 1013-1020

Gosney, W.B., Principles of Refrigeration, Cambridge University Press, UK, 1982

Hermes, C.J.L., Barbosa Jr., J.R., Thermodynamic comparison of Peltier, Stirling, and vapor compression portable coolers, Appl. Energ. 91 (2012) 51–58

Kaynakli, O., Horuz, I., An experimental analysis of automotive air conditioning system, Int. Comm. Heat Mass Transfer 30 (2003) 273-278

Shah, R.K., Automotive Air-Conditioning Systems – Historical Developments, the State of Technology, and Future Trends, Heat Transfer Engineering, 30 (2009) 720-735

Tian, C., Dou, C., Yang, X., Li, X., Instability of automotive air conditioning system with a variable displacement compressor. Part 1. Experimental investigation, Int. J. Refrig. 28 (2005) 1102-1110

Zheng, W., Chen, Y., Hua, N., Tianming, Z., Yulie, G., Comparative performance of an automotive air conditioning system using micro-channel condenser with and without liquid-vapor separation, Appl. Therm. Eng. 61 (2014) 1646-1649

9. RESPONSIBILITY NOTICE

The authors are the only responsible for the printed material included in this paper.